J Mater Sci (2011) 46:4832–4849
DOI 10.1007/s10853-011-5395-x

A1-$L1_2$ interfacial free energies from data on coarsening in five binary Ni alloys, informed by thermodynamic phase diagram assessments

Alan J. Ardell

Received: 16 October 2010 / Accepted: 12 February 2011 / Published online: 11 March 2011

Abstract The data on coarsening of γ'-type precipitates (Ni_3X, with the $L1_2$ crystal structure) in Ni–Al, Ni–Ga, Ni–Ge, Ni–Si, and Ni–Ti alloys are re-evaluated in the context of recent (TIDC) and classical (LSW) theories of coarsening, with the objective of ascertaining the best values possible of interfacial free energies, σ, of the γ/γ' interfaces in these five alloy systems. The re-evaluations include fitting of the particle size distributions, reanalyzing all the available data on the kinetics of particle growth and kinetics of solute depletion, and using thermodynamic assessments of the binary alloy phase diagrams to calculate curvatures of the Gibbs free energies of mixing. The product of the work is two sets of interfacial free energies, one set for the analysis using the recent TIDC theory and the other for the analysis using the classical LSW theory. The TIDC-based analysis yields lower values of σ by about a factor of 2/3. All the interfacial energies are considerably larger, by factors ranging from ~ 4 to 10, than those previously reported, which were for the most part calculated from data on coarsening assuming ideal-solution thermodynamics. In the TIDC theory the width of the interface, δ, is allowed to increase with particle size, r. A simple equation relating σ to the ratio of the gradient energy and δ is used to show that σ can remain constant even though δ increases with r. Published work supporting this contention is presented and discussed.

Introduction

Advances in one or more areas of research often impact the findings and conclusions drawn from analyses of data that predate these advances. The specific example in this work is the calculation of interfacial energies derived from the analyses of data on coarsening of precipitates. In the first theories of coarsening Lifshitz and Slyozov (LS) [1] and Wagner (W) [2] derived equations for the growth of a spherical particle of average radius $\langle r \rangle$. LS also derived an equation for the depletion of the small concentration of excess solute, $X_\alpha - X_{\alpha e}$, that must accompany the growth of the average precipitate; X_α is the solute concentration in the matrix at time t and $X_{\alpha e}$ is its thermodynamic equilibrium value. The kinetics of the processes of growth and solute depletion were shown to obey the equations $\langle r \rangle^3 \approx kt$ and $X_\alpha - X_{\alpha e} \approx (\kappa t)^{-1/3}$, where k and κ are rate constants that depend on the thermo-physical parameters of the alloy system, including the chemical diffusion coefficient, $\tilde{D}$, in the parent phase and the interfacial free energy, σ, between the precipitate and matrix phases. A remarkable ingredient of the LSW theory was an analytical equation describing the distribution of particle sizes (PSD). The PSD must exist as an essential component of the ensemble of particles, and its prediction was a significant advance over earlier theoretical efforts [3, 4] to describe the kinetics of growth of an ensemble of particles.

A brief history

In the original LSW theory the initial composition of the alloy, X_o, was assumed to be so small that the free energy of mixing of the solid solution was quite reasonably taken as ideal. In this case the rate constant k is given by the equation

$$k = \frac{8\sigma \tilde{D} X_{\alpha e} V_m}{9RT}, \tag{1}$$

A. J. Ardell (✉)
Division of Materials Research, National Science Foundation, Arlington, VA 22230, USA
e-mail: aardell@nsf.gov

where V_m is the partial molar volume of solute in the precipitate phase, R is the gas constant, and T is the absolute temperature.[1] In one of the earliest attempts to validate the LSW theory quantitatively, Ardell and Nicholson [5] used diffusion coefficients published in the literature to estimate the magnitude of σ for the interface between the Ni–Al solid solution (the γ phase) in equilibrium with Ni_3Al (γ') precipitates, finding it to be ~ 30 mJ/m^2.

It was soon realized [6] that if the kinetics of growth and solute depletion could be measured independently the rate constants k and κ could also be determined independently, enabling σ to be estimated without the need to know the value of $\tilde{D}$ and vice versa. Borrowing from original ideas of Ben Israel and Fine [7], and taking advantage of the very strong dependence on Al content of the ferromagnetic Curie temperature of Ni [8], the kinetics of solute depletion in Ni–Al alloys [9] were measured and the equation

$$X_\alpha - X_{\alpha e} = (\kappa t)^{-1/3} \tag{2}$$

was used to obtain the rate constant κ, which is related to the thermo-physical parameters of the system by the equation

$$\kappa = \frac{\tilde{D}(RT)^2}{9X_{\alpha e}^2 V_m}. \tag{3}$$

Straightforward manipulation of Eqs. 1 and 3 produces the result

$$\ell = \left(\frac{k}{\kappa}\right)^{1/3} = \frac{2\sigma X_{\alpha e} V_m}{RT}, \tag{4}$$

from which σ can be readily calculated. The parameter ℓ has units of length and is called the capillary length. The application of Eq. 4 to data on the kinetics of particle growth [10] and new data on the kinetics of solute depletion [6] yielded a value of $\sigma \approx 14$ mJ/m^2. This was regarded as perfectly reasonable compared to 30 mJ/m^2 because independent measurements of $\tilde{D}$ often disagree by an order of magnitude or more.

Another advance beyond the original LSW theory involved modifications to describe the coarsening of an intermetallic compound [11, 12]. This is an important quantitative issue because the LSW theory assumes that the dispersed phase consists of pure B. The most rigorous modification is that of Calderon et al. [13], which describes the coarsening of a phase that is not necessarily a terminal solid solution, and at the same time removes the limitation that the parent (matrix) phase be a dilute solid solution. The rate constant k in the theory of Calderon et al. [13] is expressed by the equation

$$k = \frac{8\tilde{D}V_m\sigma}{9G''_m\left(X_{\beta e} - X_{\alpha e}\right)^2}, \tag{5}$$

where $X_{\beta e}$ is the equilibrium concentration of solute in the precipitate (β) phase and G''_m is the curvature of the molar Gibbs free energy of mixing $G''_m = \left(d^2G_m/dX_\alpha^2\right)_{X_{\alpha e}}$, evaluated at the equilibrium concentration of the α phase. The capillary length becomes

$$\ell = \frac{2\sigma V_m}{G''_m\left(X_{\beta e} - X_{\alpha e}\right)}, \tag{6}$$

hence independent measurements of k and κ can still be used to evaluate σ and $\tilde{D}$ from data on the kinetics of coarsening.

The next attempt to evaluate σ from data on coarsening [14] was made using Eq. 6, re-analyzing the data on Ni–Al, but also adding other data on coarsening of γ'-type Ni_3Si and Ni_3Ti precipitates in binary Ni–Si and Ni–Ti alloys, respectively.[2] At the time of that work there were no reliable estimates of G''_m for the Ni–Si and Ni–Ti solid solutions, so the only option was to assume an ideal solution, in which case G''_m becomes

$$G''_m = \frac{RT}{X_{\alpha e}(1 - X_{\alpha e})} \tag{7}$$

at the equilibrium concentration of solute. On substituting Eq. 7 into Eq. 5, taking $X_{\beta e} \approx 1 >> X_{\alpha e}$, Eq. 5 reduces to Eq. 1. Since the work of Calderon et al. [13] included a thermodynamic model for the Ni–Al solid solution, it was possible to calculate G''_m for the non-ideal case. New estimates were obtained for the Ni(Al)/Ni_3Al interface (~ 8 mJ/m^2, including the influence of non-ideality), but for the other two alloys the values of σ for the Ni(Si)/Ni_3Si (10.2 mJ/m^2) and Ni(Ti)/Ni_3Ti (13 mJ/m^2) interfaces were calculated assuming ideal-solution thermodynamics.

Recent developments

Subsequent to the work published in 1995 [14] there have been several developments that directly impact the values of σ. Data on the kinetics of coarsening of γ'-type precipitates, including the kinetics of particle growth and solute depletion, have been published for Ni–Ga [15, 16] and Ni–Ge [17, 18] alloys. Thermodynamic models of the Ni-rich solid solutions have been published for all five

[1] In the original LSW theory no distinction was made between various kinds of diffusion coefficients. It was unnecessary because the solution was assumed to be very dilute, in which case the tracer and chemical diffusion coefficients are equal.

[2] Ni_3Si and Ni_3Ti both exist with the $L1_2$ crystal structure. The Ni_3Si phase is stable and is called β_1. Ni_3Ti is metastable. The stable phase is called η and has the hexagonal DO_{24} crystal structure.

binary alloy systems: Ni–Al [19–21], Ni–Ga [22], Ni–Ge [23], Ni–Si [24–26], and Ni–Ti [27]. There are also thermodynamic models of ternary Ni-rich solid solutions involving Al, Ga, Ge, Si, and Ti that are helpful in selecting data on G_m [28–33]. As discussed recently by Costa e Silva et al. [34], the deviation from ideality can have a significant effect on the values of σ derived from data on coarsening, invariably increasing them because G''_m increases as the departure from ideal solution behavior increases. Though this is quite evident from Eqs. 5 and 6, the discussions of Costa e Silva et al. on σ in Ni–Al and other alloys forcefully drive home the point.

Two other important factors have had a dramatic impact on the validity of the LSW theory itself under certain circumstances, and therefore whether it can be used without further modification to extract meaningful values of σ and $\tilde{D}$ from data on coarsening. The first factor involves puzzling observations on the effect of equilibrium volume fraction, f_e, on the kinetics of coarsening in all the aforementioned binary Ni alloys—there is simply no effect of f_e when f_e exceeds ~ 0.08 or so.[3] The conundrum arises from the theoretically sound expectation that when coarsening kinetics is diffusion-controlled, the rate constants k and κ should increase as f_e increases; discussions can be found in several review articles [35–38].

The second important factor is that the γ/γ' interface in Ni–Al alloys is not sharp, but diffuse, the transition from the γ' to the γ phase in planar interfaces occurring over a distance of ~ 2 nm. The first evidence for this was reported by Harada et al. [39]. This early observation has been confirmed by atomistic modeling [40], recent experimental observations using modern atom-probe tomography [41] and high-resolution transmission electron microscopy [42]. A reconciliation of these findings, i.e., the independence of the rate constants on f_e and the diffuse γ/γ' interface, provided the stimulus for a new theory of coarsening by Ardell and Ozolins [43], who also showed that the interface is not only diffuse, but also quite ragged in structure. Ardell and Ozolins postulated that chemical diffusion through the interface controls the kinetics of coarsening when diffusion *through* the interface is slower than diffusion *to* the interface. This condition can prevail in Ni–Al alloys because diffusion in the ordered γ' phase is generally much slower than diffusion in the disordered matrix [44–47]. The γ/γ' interface thus becomes a bottleneck for diffusion, with significant consequences for the kinetics, leading to the so-called Trans-Interface-Diffusion-Controlled (TIDC) theory of coarsening. The consequences of the TIDC theory in obtaining values of σ from data on coarsening are described in the following sections.

The TIDC theory—quantitative predictions

The important predictions of the TIDC theory are that the kinetics of growth and solute depletion are given by the equations $\langle r\rangle^n \approx k_T t$ and $X_\alpha - X_{\alpha e} \approx (\kappa_T t)^{-1/n}$ where n is an exponent that satisfies the condition $2 < n < 3$. The rate constants k_T and κ_T are expressed as [48]

$$k_T = \left(\frac{n-1}{n}\right)^{(n-1)} \frac{r_{min}^m \langle u\rangle^n \tilde{D}_I \ell_T}{a_o \Delta X_e} \tag{8}$$

and

$$\kappa_T = \left(\frac{n-1}{n}\right)^{n} \frac{r_{min}^m \tilde{D}_I}{a_o \Delta X_e \ell_T^{n-1}}. \tag{9}$$

The parameter r_{min} is the radius of a particle of minimum size and a_o is a lattice constant. They are related to the radius, r, of the particle and the width of the interface, δ, by the equation

$$\delta = a_o \left(\frac{r}{r_{min}}\right)^m; \tag{10}$$

r_{min} is a radius below which Eq. 10 is no longer valid. The exponent m satisfies the conditions $0 < m < 1$ and $n = m + 2$. The other parameters in Eqs. 8 and 9 are $\tilde{D}_I$, the chemical diffusion coefficient in the interface, $\Delta X_e = X_{\beta e} - X_{\alpha e}$ and the capillary length in the TIDC theory, which is expressed by the equation

$$\ell_T = \frac{1}{\langle u\rangle}\left(\frac{k_T}{\kappa_T}\right)^{1/n}, \tag{11}$$

where $\langle u\rangle = \langle r\rangle/r^*$ and r^* is a critical radius; particles of size $r = r^*$ are neither growing nor shrinking at time t. In the original LSW theory $\langle u\rangle = 1$, but in the TIDC theory $\langle u\rangle < 1$. The interfacial free energy in the TIDC theory is calculated from the equation

$$\sigma = \frac{\Delta X_e G''_m}{2V_m\langle u\rangle}\left(\frac{k_T}{\kappa_T}\right)^{1/n}, \tag{12}$$

which is obtained from Eqs. 8 and 9 by straightforward algebraic manipulation.

The exponent n in the TIDC theory dictates the shape of the PSDs through the function $h(z)$, expressed in terms of the variable $z = r/r^*$, which is given by the equation

$$h(z) = -3f(z)exp\{p(z)\}, \tag{13}$$

where $p(z)$ is the function

[3] The rate constants for coarsening in all five alloys actually decrease as f_e increases when f_e is very small ($f_e < 0.05$). This anomalous behavior awaits a satisfactory explanation.

$$p(z) = \int_0^z f(x)\mathrm{d}x, \tag{14}$$

and $f(z)$ is related to z by the expression

$$f(z) = \frac{z^{(n-1)}}{(z-1)\frac{n^n}{(n-1)^{(n-1)}} - z^n}. \tag{15}$$

For comparison with experimentally determined PSDs it is necessary to use the function $g(u)$, where $u = r/\langle r\rangle$ and $g(u) = \langle u\rangle h(z)$. The maximum allowable scaled particle size in the distribution, $u_{\max}$, is

$$u_{\max} = \frac{n}{n-1}. \tag{16}$$

A restriction of the TIDC theory is that it should no longer be valid for particles larger than a transitional particle size, r_T, defined by the condition $r_T \geq \delta\tilde{D}/\tilde{D}_I$ [43]. At such large sizes the flux of solute in the matrix to the interface is slower than the flux of solute through the interface, so the kinetics of coarsening become controlled by chemical diffusion in the matrix, i.e., LSW coarsening should prevail at larger particle sizes, or equivalently, longer aging times. In the Ni–Al, Ni–Ga, and Ni–Ti alloy systems the restriction does not apply because elastic interactions induce severe departures from equiaxed shapes at relatively small sizes ($r < 20$ nm). These interactions generally prevent meaningful average radii larger than this from being measured. Such is not the case for Ni–Si and Ni–Ge alloys, in which Ni_3Si and Ni_3Ge precipitates can grow large enough for the transition from TIDC to LSW kinetics to take effect. This will be evident in the following analyses of the data.

Examination of the data on binary Ni alloys

In this section data on the PSDs of γ'-type precipitates in binary Ni–Al, Ni–Ga, Ni–Ge, Ni–Si, and Ni–Ti alloys are re-examined for the purpose of determining the values of n used subsequently to re-examine the data on kinetics of particle growth and solute depletion. The rate constants k_T and κ_T can then be extracted from the data and used to calculate σ via Eq. 12. As in previous work [43, 48, 49], a Mathematica subroutine was fitted to the experimental data on the PSDs in a least-squares sense using trial values of n until the value of n producing the smallest deviation was found. In most, but not all, cases it was possible to obtain a value of n satisfying the condition $2 \leq n \leq 3$; only these values of n were used in the subsequent analyses. The main significant procedural difference between this and previous work is that populations of data (aging times at a specific temperature) were evaluated individually, yielding average values of n with their variances, which were then used to calculate the average values for all populations. For example, the PSDs of γ' precipitates in Ni–Al alloys reported by Ardell and Nicholson [10] for their three aging conditions, and those reported by Jayanth and Nash [50] and Irisarri et al. [51], were all evaluated as individual populations, each of which produced an average value of n with its own variance. Previously, the values of n obtained by fitting the individual PSDs were averaged irrespective of source and aging conditions. The average values of n differ slightly, but the new procedure provides more statistically significant results. The collective PSDs of Ardell and Nicholson [10] are shown in Fig. 1a and the PSDs of Jayanth and Nash [50] and Irisarri et al. [51] are shown in Fig. 1b.

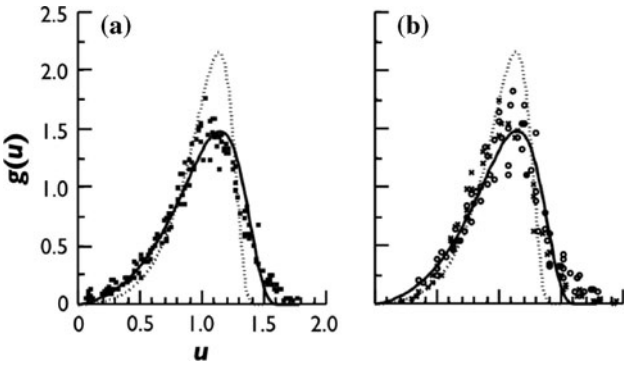

Fig. 1 Fitting of the γ' particle size distributions in Ni–Al alloys. The data of Ardell and Nicholson [10] are shown in **a**. The data of Jayanth and Nash [50] (*cross*) and Irisarri et al. [51] (*circle*) are shown in **b**. The *solid curves* show the PSD of the TIDC theory for $n = 2.424$ and the *dashed curves* show the PSD of the LSW theory

The data on the other four binary alloys were taken from the following sources: Ni–Ga [15, 16], Ni–Ge [17, 18], Ni–Si [52], and Ni–Ti [49]. The fits to the collective data on each alloy are shown in Fig. 2. The theoretical PSDs of the TIDC and LSW theories are shown in each plot in Figs. 1 and 2. In the case of Ni–Al the data clearly indicate that the fit to the TIDC is better than for the LSW theory. This is not so obvious for the other alloys for a variety of different reasons. One is that the counting statistics were much better for Ni–Al: Ardell and Nicholson [10] measured more than 400 particles, Jayanth and Nash [50] measured over 1000 particles and Irisarri et al. [51] measured 350 particles on average. For many of the other sets of data fewer than 300 particles were counted, so the spread in the values of $g(u)$ at any given value of u is far larger for the other alloys than for Ni–Al. It is also the case for the Ni–Ga and Ni–Ti alloys that the γ' precipitates interact very strongly [15, 16], which makes measurements at longer aging times more difficult as the particles deviate increasingly from an equiaxed shape. This, combined with

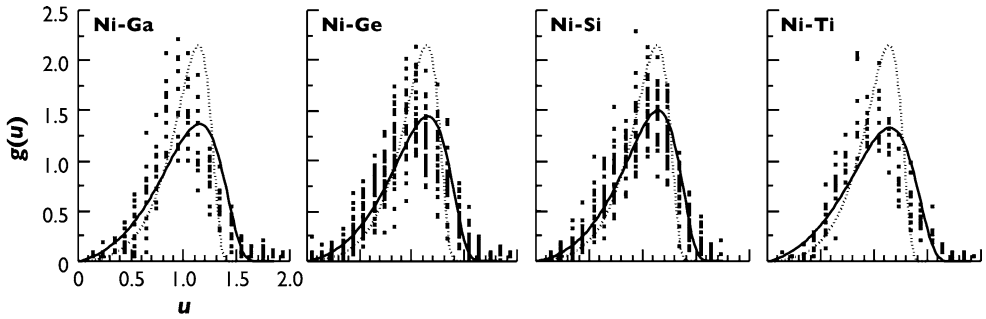

Fig. 2 Fitting of the particle size distributions of the γ'-type precipitates in Ni–Ga, Ni–Ge, Ni–Si, and Ni–Ti alloys. A few data points for $u > 2$ have been omitted, and some of the data have been omitted for clarity. The *solid curves* show the PSDs of the TIDC theory for $n = 2.318$ (Ni–Ga), $n = 2.385$ (Ni–Ge), $n = 2.444$ (Ni–Si), and $n = 2.281$ (Ni–Ti). The *dashed curves* are the PSD of the LSW theory

the smaller number of particles counted at larger particle sizes, increases the uncertainties in the PSDs and results in more uncertain values of n. As was the case for the Ni–Ti alloys re-examined previously [49], there were Ni–Ga PSDs that could not be fitted (2 for the data of Kim and Ardell [15], 3 for the data of Wimmel and Ardell [16]) and one Ni–Ge PSD that could not be fitted [18].

The values of n resulting from the averaging method used, and their standard deviations, are summarized in Table 1. The values of n are reported to three significant figures, which belies the accuracy of the measurements. Nevertheless, they are represented this way, as are the values of other parameters calculated from the data, to enable the interested reader to check the validity of the calculations in this work. The rate constants k_T and κ_T were obtained for all the alloys by plotting the data on kinetics using the equations $\langle r\rangle^n \approx k_T t$ and $X_\alpha - X_{\alpha e} \approx (\kappa_T t)^{-1/n}$. As is evident from the work of Ardell and Ozolins [43], the fits to the data on coarsening of γ' precipitates in Ni–Al are nearly as good using $n = 2$ as they are with $n = 3$, and as shown more recently by Ardell [48] the comparison is even better for $n = 2.4$. The same is true for the data on all the other alloys using the values of n in Table 1. The data on each alloy are considered in turn.

Table 1 Values of the exponent n and average values of $\langle u\rangle = \langle r\rangle/r^*$ resulting from fitting the PSDs measured experimentally in the Ni–Al, Ni–Ga, Ni–Ge, Ni–Si, and Ni–Ti alloys

Alloy	n	$\langle u\rangle$
Ni–Al	2.424 ± 0.089	0.9537
Ni–Ga	2.318 ± 0.164	0.9409
Ni–Ge	2.385 ± 0.095	0.9492
Ni–Si	2.444 ± 0.086	0.9559
Ni–Ti	2.281 ± 0.069	0.9359

Ni–Al

The data on coarsening of γ' precipitates in the context of the TIDC theory were analyzed recently by Ardell [48], so there is little to add here other than that the slightly different method of averaging produced a slightly higher value of $n = 2.424$ compared to the previous $n = 2.4$.

Ni–Ga

The data of Kim and Ardell [15] and Wimmel and Ardell [16], analyzed in the context of the TIDC theory, are shown in Fig. 3 (kinetics of particle growth) and Fig. 4 (kinetics of solute depletion). Kim and Ardell measured the kinetics of solute depletion only for the alloy containing 18.31% Ga. The microstructure of the aged alloy contained many non-equiaxed Ni_3Ga particles, so only the data for the smallest three aging times were used in the present analysis, as was the case originally [15]; i.e., the data in Fig. 3a correspond to the first three data points in Fig. 4 of Kim and Ardell [15]. It is not shown here, but the kinetics is described equally well by the TIDC ($n = 2.318$) and LSW theories.

Ni–Ge

The data of Kim and Ardell [17] and Wimmel and Ardell [18] on the kinetics of particle growth, analyzed in the context of the LSW and TIDC ($n = 2.385$) theories, are shown in Fig. 5. It is apparent in Fig. 5b that the linear fit in the TIDC analysis is excellent up to $t \approx 1.1 \times 10^5$ s, but there is significant deviation at longer aging times. The average "radius", or half edge length, of the cuboidal-shaped particles at this aging time is 70–75 nm. It is postulated here that the radius of 70–75 nm corresponds to the transition radius $r_T \geq \delta\tilde{D}/\tilde{D}_I$ of the TIDC theory and that LSW coarsening should prevail for $\langle r\rangle > r_T$. An estimate of r_T will be postponed for now, but the interpretation

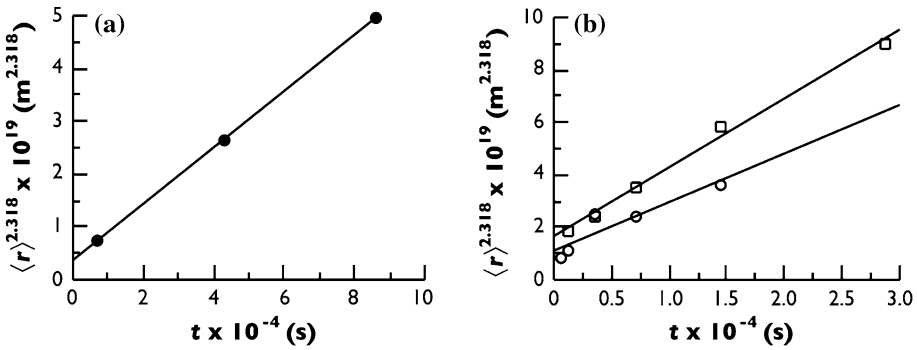

Fig. 3 Data on the kinetics of particle growth of Ni_3Ga precipitates, plotted as average radius to the 2.318 power, $\langle r \rangle^{2.318}$, vs. aging time, t: **a** data of Kim and Ardell [15], aging temperature = 628 °C, 18.31% Ga; **b** data of Wimmel and Ardell [16], aging temperature = 700 °C, *open circles* 15.70% Ga, *open squares* 16.44% Ga

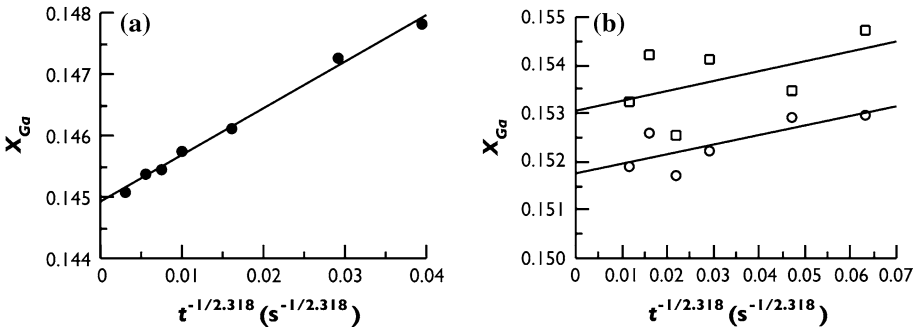

Fig. 4 Data on the kinetics of solute depletion during coarsening of Ni_3Ga precipitates, plotted as solute concentration, X_{Ga} vs. aging time to the −1/2.318 power, $t^{-1/2.318}$: **a** Data of Kim and Ardell [15], **b** data of Wimmel and Ardell [16]. The alloys, aging conditions, and plotting symbols are identical to those described in Fig. 3

offered here is that the data used to obtain both k_T and κ_T are limited to particle "radii" below 70 nm in Ni–Ge alloys. Though not shown specifically, the linear fits to the data in Fig. 5b ($n = 2.385$) are actually better than the fits to the data in Fig. 5a ($n = 3$).

The kinetics of solute depletion is shown in Figs. 6 and 7. Figure 6 shows the data of Kim and Ardell [17], excluding data on aging times for which $\langle r \rangle > 70$ nm, while Fig. 7 shows the data of Wimmel and Ardell [18]. In the latter investigation the average particle radius never exceeded 28 nm, so all the data are included in the analysis. The kinetics of particle growth for the data of Wimmel and Ardell are not shown because there is no additional point to be made by showing them; the fits of these data to plots of $\langle r \rangle^{2.385}$ vs. t and $\langle r \rangle^3$ vs. t are comparable.

Ni–Si

There are several sets of data on the coarsening of Ni_3Si precipitates in binary Ni–Si alloys that can be used to calculate σ. Two of these, the aforementioned results of Rastogi and Ardell [52] and data of Polat et al. [53], were analyzed previously [54] and shown to yield results in reasonably good agreement, the data of Polat et al. producing somewhat larger values using an analysis based on LSW kinetics. The data on kinetics considered here are those of Rastogi and Ardell and Cho and Ardell [55].

The data of Rastogi and Ardell on the kinetics of particle growth are shown in Fig. 8, while Fig. 9 shows the data on the kinetics of solute depletion. The data on the kinetics of particle growth are described slightly better by the TIDC theory, Fig. 8b, while the kinetics of solute depletion are described essentially equally well by the LSW and TIDC theories, Fig. 9. The marked deviation from linearity seen in Fig. 9 is associated by the loss of coherency of the Ni_3Si precipitates at the rather high aging temperature used by Rastogi and Ardell [52]. The largest particle radius plotted in Fig. 8 is ~75 nm, obtained after 8 h at 775 °C. The three data points that deviate from linearity in Fig. 9 represent measurements taken after 16 h of aging; Rastogi and Ardell [52] showed examples of semicoherent Ni_3Si precipitates observed at these longer aging times.

The data of Cho and Ardell [55] on four alloys aged at 650 °C are shown in Figs. 10 and 11. The largest particles observed at the longer aging times ($t > 60$ h) had average radii exceeding 80 nm, but at this aging temperature the particles were, nevertheless, fully coherent. The data are reasonably well described by the LSW theory, as seen in Fig. 10a, though they exhibit a perceptible negative curvature. When the data are plotted for consistency with the TIDC theory, Fig. 10b, there is a significant departure from linearity seen at aging times exceeding $\sim 2 \times 10^6$ s, which corresponds to $\langle r \rangle \approx 80$ nm. The precipitate microstructures for Ni_3Si resemble those of Ni_3Ge in that neither coalescence nor impingement is ever observed. As is the case for Ni_3Ge precipitates, it is postulated that the average radius of the larger Ni_3Si precipitates exceeds the transition radius, r_T, and that LSW coarsening kinetics obtain for

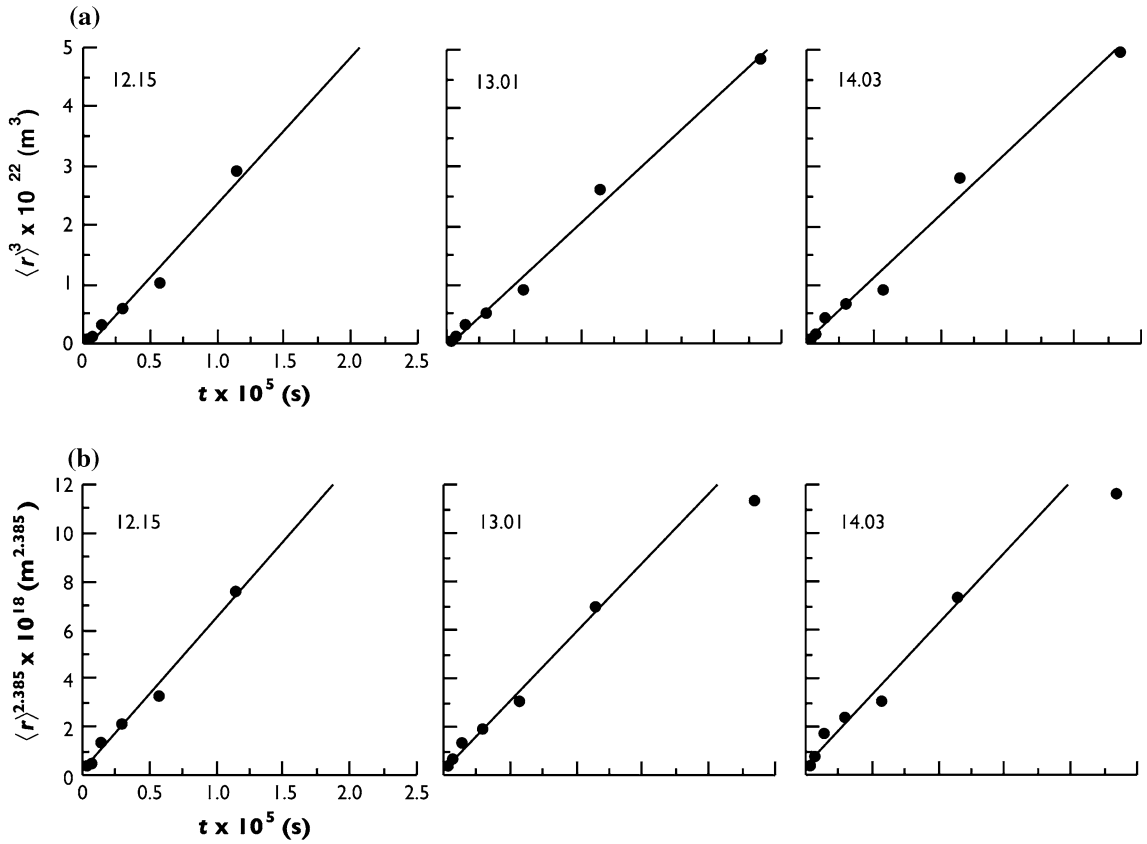

Fig. 5 Data of Kim and Ardell [17] on the kinetics of particle growth of Ni_3Ge precipitates at 724 °C: **a** plotted as average radius, $\langle r \rangle^3$ vs. aging time t for consistency with the LSW theory; **b** plotted as $\langle r \rangle^{2.385}$ vs. aging time, t, for consistency with the TIDC theory. The compositions of the alloys are inset in each figure

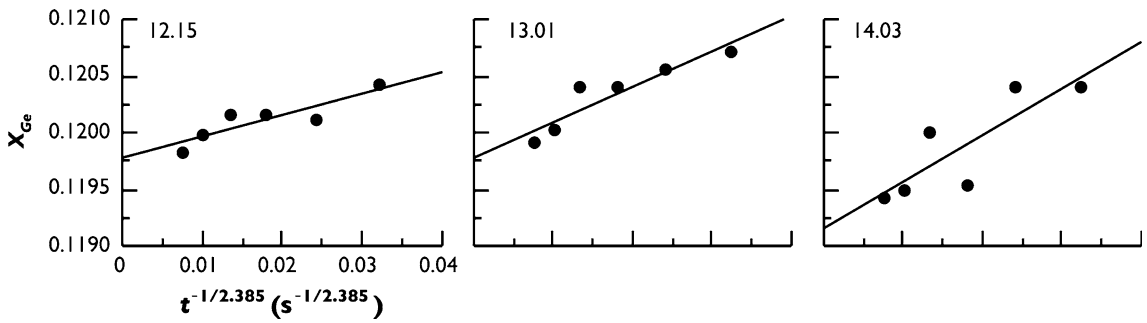

Fig. 6 Data of Kim and Ardell [17] on the kinetics of solute depletion during coarsening of Ni_3Ge precipitates at 724 °C, plotted as solute concentration, X_{Ge} vs. aging time to the −1/2.385 power, $t^{-1/2.385}$. The compositions of the alloys are inset in each figure

$\langle r \rangle > r_T \approx 80$ nm. Subsequent analysis involving the TIDC theory uses only the data incorporated in the linear fits in Fig. 10b.

The kinetics of solute depletion is shown in Fig. 11, plotted for consistency with the predictions of the TIDC theory. The fits with plots of X_{Si} vs. $t^{-1/3}$ are comparable. The data in Fig. 11 represent aging times for which $\langle r \rangle < 80$ nm, so all the data are included in the linear fitting.

Ni–Ti

The kinetics of coarsening of Ni_3Ti precipitates has been investigated by Ardell [56] and Kim and Ardell [57]. These data were evaluated according to the predictions of the TIDC theory by Ardell et al. [49], so the figures will not be reproduced here. The main difference between the evaluation of the data by Ardell et al. and this work is that the value of n is somewhat lower; $n = 2.281$ cf. 2.375. This is

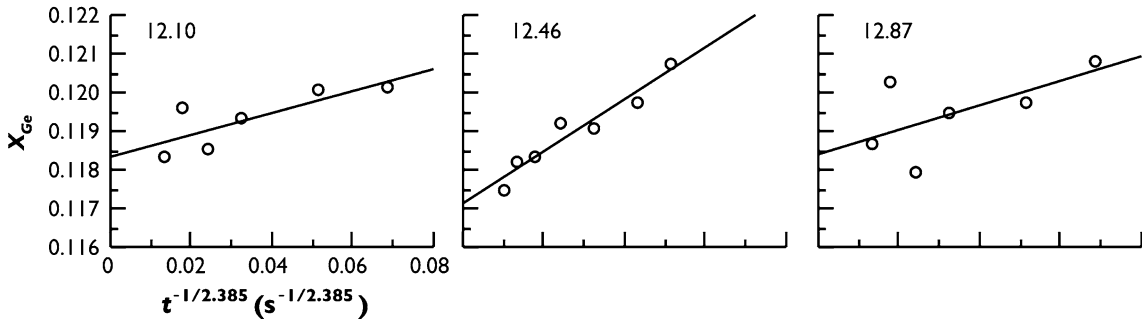

Fig. 7 Data of Wimmel and Ardell [18] on the kinetics of solute depletion during coarsening of Ni_3Ge precipitates at 700 °C, plotted as average solute concentration, X_{Ge}, vs. aging time to the −1/2.385 power, $t^{-1/2.385}$. The compositions of the alloys are inset in each figure

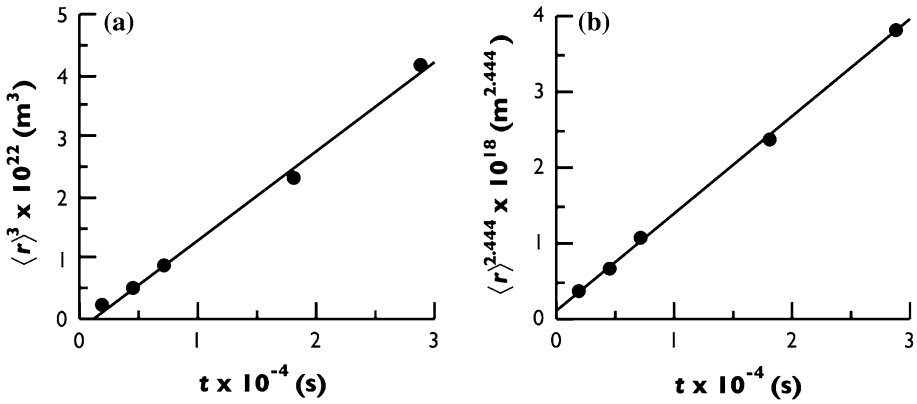

Fig. 8 The data of Rastogi and Ardell [52] on the kinetics of particle growth of Ni_3Si precipitates in a Ni–12.68% Si alloy aged at 775 °C: **a** plotted as the cube of the average radius, $\langle r \rangle^3$ vs aging time, t, for consistency with the LSW theory; **b** plotted as $\langle r \rangle^{2.444}$ vs. t for consistency with the TIDC theory

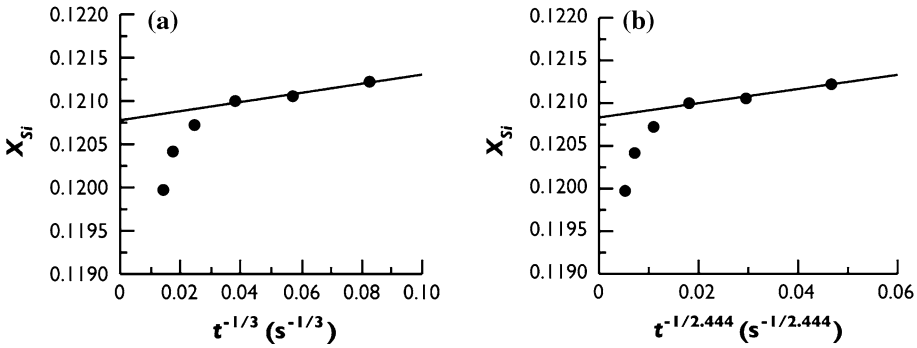

Fig. 9 The data of Rastogi and Ardell [52] on the kinetics of solute depletion during coarsening of Ni_3Si precipitates in a Ni–12.68% Si alloy aged at 775 °C: **a** plotted as solute concentration in the matrix, X_{Si}, vs. aging time to the −1/3 power, $t^{-1/3}$, for consistency with the LSW theory; **b** plotted as X_{Si} vs. $t^{-1/2.444}$ for consistency with the TIDC theory

due partly to the inclusion of the data for $t = 4$ h, partly to the way the average value of n was calculated and partly due to a minor change in the conversion of the original histograms to the representation shown in Fig. 2. The fits to the data for $n = 2.281$ are comparable to those seen in the paper by Ardell et al. [49].

Thermodynamics

Curvatures of the free energy functions

The calculations of σ for the five alloys using Eq. 12 require estimates of G''_m. Values of σ can then be obtained from the experimental data on the rate constants using the appropriate rate constants from either the LSW or TIDC theories. Fortunately, the five alloy systems relevant here have been subjected to thermodynamic assessments with the objectives of describing the phase diagrams and their thermodynamic properties using a variety of experimental data; this is the essence of the CALPHAD method. These assessments require, as input, equations describing the Gibbs free energies of mixing, G_m, as functions of compositions for all the phases. For this work all that is needed are the equations describing G_m for the terminal γ solid solution phases as functions of composition and temperature. The necessary differentiations can then be performed to obtain G''_m evaluated at their appropriate equilibrium compositions.

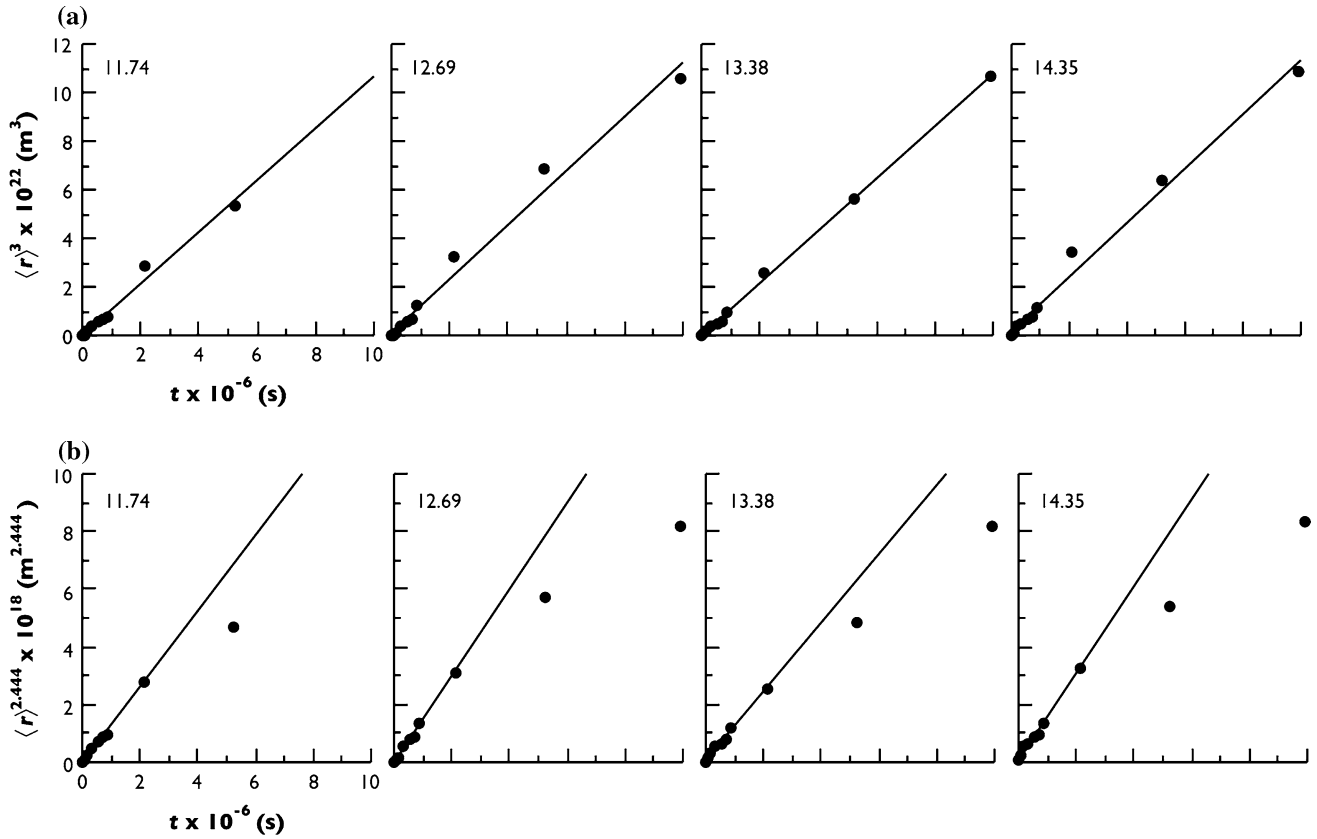

Fig. 10 Data of Cho and Ardell [55] on the kinetics of particle growth of Ni_3Si precipitates at 625 °C: **a** plotted as average radius, $\langle r \rangle^3$ vs. aging time t for consistency with the LSW theory; **b** plotted as $\langle r \rangle^{2.444}$ vs. aging time t for consistency with the TIDC theory. The compositions of the alloys are inset in each figure

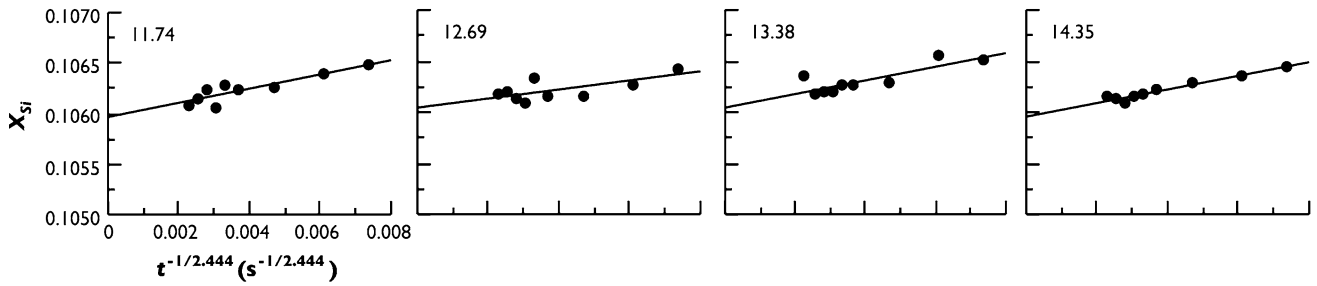

Fig. 11 Data of Cho and Ardell [55] on the kinetics of solute depletion during coarsening of Ni_3Si precipitates at 625 °C, plotted as solute concentration in the matrix, X_{Si}, vs. aging time to the -1/2.444 power, $t^{-1/2.444}$. The compositions of the alloys are inset in each figure

The Gibbs free energy of mixing is given by the sum of three terms,

$$G_m = G_{m,id} + G_{m,exc} + G_{m,mag}, \quad (17)$$

where $G_{m,id}$ is the free energy of mixing of an ideal solution, $G_{m,exc}$ is the excess free energy of mixing and represents the departure from ideal solution behavior of the solid solution and $G_{m,mag}$ is an additional contribution to the free energy that exists when the majority phase is ferromagnetic [58]. This contribution exists even above the ferromagnetic Curie temperature, T_C, [59, 60] and can be important, in principle. Equations for the second derivatives with respect to composition for each of these quantities will be presented in turn.

The second derivative of $G_{m,id}$, Eq. 7, is valid for any value of X, not just at thermodynamic equilibrium. In all subsequent equations X represents the concentration of solute; subscripts identifying the solute will be added as needed.

The excess free energy in the lexicon of thermodynamic assessments of phase diagrams is universally represented by the Redlich–Kister [61] equation, which is written here in the form

$$G_{\mathrm{m,exc}} = X(1-X)L_{\mathrm{RK}}, \tag{18}$$

where L_{RK} is a summation that takes one of two forms for an A–B binary solid solution, depending on whether or not the elements A and B are represented alphabetically in the thermodynamic modeling scheme. This seems like a trivial issue, but for the researcher who is unaccustomed to probing the literature on thermodynamic modeling, and must rely on the equations to understand its predictions, the wrong choice can lead to completely erroneous results. Since A and B are not universally chosen alphabetically, the equations for L_{RK} are presented here for the two possible cases.

Case 1:

$$L_{\mathrm{RK}} = \sum_{j=0} (X_{Ni} - X)^j L_j = \sum_{j=0} (1-2X)^j L_j \tag{19a}$$

Case 2:

$$L_{\mathrm{RK}} = \sum_{j=0} (X - X_{\mathrm{Ni}})^j L_j = \sum_{j=0} (2X-1)^j L_j \tag{19b}$$

The coefficients L_j in the sums depend only on T and are obtained by fitting the free energy functions to the phase boundaries in the phase diagrams and other relevant available data.

For both cases the curvature of the excess free energy is given by the equation

$$G''_{\mathrm{m}} = -2L_{\mathrm{RK}} + 2(1-2X)L'_{\mathrm{RK}} + X(1-X)L''_{\mathrm{RK}}, \tag{20}$$

where the prime and double prime indicate second derivatives with respect to X. The expressions for the derivatives of L_{RK} depend on whether Case 1 or Case 2 applies. For the alloys considered in this work the thermodynamic models involve at most four terms in the summations in Eq. (19). The equations for the derivatives in Cases 1 and 2 are therefore expressed as follows:

Case 1:

$$L'_{\mathrm{RK}} = -2\Big\{L_1 + 2(1-2X)L_2 + 3(1-2X)^2 L_3\Big\} \tag{21a}$$

$$L''_{\mathrm{RK}} = 8\{L_2 + 3(1-2X)L_3\} \tag{21b}$$

Case 2:

$$L'_{\mathrm{RK}} = 2\Big\{L_1 + 2(2X-1)L_2 + 3(2X-1)^2 L_3\Big\} \tag{22a}$$

$$L''_{\mathrm{RK}} = 8\{L_2 + 3(2X-1)L_3\} \tag{22b}$$

The magnetic contribution to the free energy is expected to be small, since T_{C} for the Ni–Al, Ni–Ga, Ni–Ge, Ni–Si, and Ni–Ti alloys decreases sharply with composition (see [9, 16, 18, 52, 56] and references therein for representative dependencies of T_{C} on X), and the aging temperatures in the experiments on coarsening significantly exceeded T_{C}. Nevertheless, it is at least worthwhile to calculate $G''_{\mathrm{m,mag}}$ to see if neglecting its contribution is justifiable. It is shown in the Appendix 1 that this contribution is negligibly small.

Thermodynamic models and equilibrium solubility limits of the γ and γ' phases

Equations describing the L_j obtained from the thermodynamic assessments of the five phase diagrams are presented in Table 2. For the Ni–Ti alloy system the thermodynamic models involve equilibrium between the f.c.c. Ni–Ti solid solution and the hexagonal ordered η phase whereas the data on coarsening involve the metastable $L1_2$ Ni_3Ti phase. The function describing the free energy of the f.c.c. solid solution is, of course, unaffected.

The remaining parameters needed to calculate σ using the equations of either the LSW or TIDC theories are the equilibrium solubility limits of both the γ and γ' phases and the partial atomic volumes. As to the solubility limits, there are many options to choose from, since there are contributions to the phase diagrams from numerous investigators. The values of $X_{\gamma\mathrm{e}}$ (= $X_{\alpha\mathrm{e}}$) chosen here were obtained from data on the kinetics of solute depletion, plotted according to the LSW version, Eq. 2, where extrapolation to $t^{-1/3} = 0$ provides a value of $X_{\gamma\mathrm{e}}$. As pointed out by Rastogi and Ardell [14], the equilibrium solubility limits so obtained represent the solubilities of the coherent precipitates. These do not necessarily differ much from the incoherent solubility limits, but it seems a reasonable choice to use them. In the case of the $L1_2$ form of the Ni_3Ti phase, the only other measurements of its solubility limits are those of Hashimoto and Tsujimoto [62], which agree well with those of Rastogi and Ardell. It is important to

Table 2 Equations for the L_j (J/mol) of the f.c.c. solid solutions in the thermodynamic assessments of the binary Ni–Al, Ni–Ga, Ni–Ge, Ni–Si, and Ni–Ti phase diagrams

Alloy	Source	Case	L_j (J/mol)
Ni–Al	Ansara et al. [19]	2	L_0 –162,407.75 + 16.212965 T
			L_1 73,417.798 – 34.914 T
			L_2 33,471.014 – 0.837 T
			L_3 –30,758.01 + 10.253 T
Ni–Ga	Yuan et al. [22]	1	L_0 –130,526 + 40 T
Ni–Ge	Liu et al. [23]	2	L_0 –91,312 + 11.452 T
			L_1 120,929 – 45.241 T
Ni–Si	Tokunaga et al. [26]	1	L_0 –208,234.46 + 44.14177 T
			L_1 –108,533.44
Ni–Ti	De Keyzer et al. [24]	1	L_0 –98,143 + 6.706 T
			L_1 –62,430

The temperature T is in K. The column "Case" refers to whether Eqs. 21 or 22 should be used to substitute into Eq. 20 to calculate G''_{m}

point out that when the same data on the kinetics of solute depletion are analyzed using the counterpart to Eq. 2 in the TIDC theory, the values of $X_{\gamma e}$ so obtained are very slightly smaller than those obtained from the LSW analysis; the typical difference is less than 0.01% and is ignored in this work.

With the exception of the solvus curve for $L1_2$ Ni_3Ti precipitates, equations for the solvus curves of all the other alloys have been summarized previously [63]. These equations are presented in Table 3. The equation for the solubility limit of Ni_3Ti used here is the one published by Rastogi and Ardell [14].

The values of $X_{\beta e} = X_{\gamma' e}$ for the Ni–Al and Ni–Ge systems are calculated from equations that describe the $(\gamma + \gamma')/\gamma'$ phase boundaries in these two alloys. The equation for the Ni–Al alloy system is taken from the work of Ma and Ardell [64]:

$$X_{Ni_3Al} = 0.16 + 4.026 \times 10^{-4} T - 7.7 \times 10^{-7} T^2 + 5.8 \times 10^{-10} T^3 - 1.505 \times 10^{-13} T^4, \quad (23)$$

where T is in °C. The corresponding equation for the Ni–Ge system is

$$T = 1.3382 \times 10^6 - 1.7282 \times 10^7 X_{\gamma' e} + 7.4494 \times 10^7 X_{\gamma' e}^2 - 1.0711 \times 10^8 X_{\gamma' e}^3. \quad (24)$$

Equation 24, in which T is in °C, is somewhat awkward, but produces an excellent fit to the combined data of Ma and Ardell (unpublished research) and Ikeda et al. [65]. The data on $X_{\gamma' e}$ for Ni_3Ga, Ni_3Si, and Ni_3Ti indicate that there is no change, or at best only a small variation, of concentration with temperature. The values used here are taken from Ikeda et al. [65] (Ni_3Ga), Oya and Suzuki [66] (Ni_3Si), and Jia et al. [67] (Ni_3Ti). Jia et al. actually measured the concentration of the equilibrium η phase, which is essentially constant at ~23.2% Ti over the temperature range 700–900 °C. Other measurements indicate that the $L1_2$ form of Ni_3Ti is hypostoichiometric, with a composition of ~22 ± 2% Ti [68–70]. The value of $X_{\gamma' e}$ for the metastable Ni_3Ti $L1_2$ phase is not known precisely, and is taken here as temperature-independent and slightly smaller than that of the η phase, specifically 23.0% Ti. The values of $X_{\gamma' e}$ used in all the calculations of σ are summarized in Table 4.

The partial molar (atomic) volumes of the solute atoms in the γ'-type phases were calculated from the equilibrium lattice constants at the relevant temperatures using the relationship $V_m = a_o^3 N_A/4$, where N_A is Avogadro's number. For Ni_3Al, Ni_3Ga, Ni_3Ge, and Ni_3Si the lattice constants were taken from the data of Kamara et al. [71]. These data take thermal expansion into account, but not the variations of equilibrium composition with T, so Vegard's law was assumed to apply and corrections for variations with composition were assumed (Ardell, unpublished research). The values of V_m so obtained are summarized in Table 4. The numbers shown in Table 4 differ slightly from those published previously because of the variations of a_o with temperature and composition that were not considered in previous work.

The only measurements of the lattice constants of $L1_2$ Ni_3Ti are those of Hashimoto and Tsujimoto [62]. Their reported lattice constants decrease slightly with increasing temperature over the range 600–900 °C. They suggest that this is due to a variation in composition of the Ni_3Ti phase from ~14.2% (900 °C) to 17.1% (600 °C) Ti, but their suggestion is based on very old data on the variation of lattice constant with composition. It is worth pointing out that at the aging temperature of 600 °C the data of Hashimoto and Tsujimoto indicate that the lattice mismatch between $L1_2$ Ni_3Ti and the matrix phase is ~0.84%, which agrees well with the room-temperature value reported by Sass et al. [72]. This suggests that the compositions

Table 3 Equations representing the solvus curves for the γ'-type phases in the Ni–Al, Ni–Ga, Ni–Ge, Ni–Si, and Ni–Ti alloy systems

Alloy	$X_{\gamma e}$
Ni–Al	$5.5027 \times 10^{-2} \exp\{8.124 \times 10^{-4}\ T\}$
Ni–Ga	$7.9824 \times 10^{-2} \exp\{6.606 \times 10^{-4}\ T\}$
Ni–Ge	$5.8270 \times 10^{-2} \exp\{7.186 \times 10^{-4}\ T\}$
Ni–Si	$4.6651 \times 10^{-2} \exp\{8.911 \times 10^{-4}\ T\}$
Ni–Ti	$0.2566 \exp\{-1850/RT\}$

$X_{\gamma e}$ is the equilibrium solubility in atom fraction and T is the temperature in K

Table 4 Thermodynamic variables used in the calculation of σ at the various temperatures, T, used in the experiments on coarsening: V_m is the partial atomic volume; $X_{\gamma e}$ and $X_{\gamma' e}$ are the equilibrium solute concentrations in the γ and γ' phases, respectively; G''_m is the second derivative of the total Gibbs free energy of mixing in the γ phase, evaluated at the equilibrium compositions of the γ phase at each temperature

Alloy	T (K)	$V_m \times 10^6$ (m^3/mol)	$X_{\gamma e}$	$X_{\gamma' e}$	G''_m (J/mol)
Ni–Al	898	7.0345	0.1141	0.2295	339,194
Ni–Al	988	7.0633	0.1228	0.2269	346,735
Ni–Ga	901	7.1968	0.1448	0.2327	249,480
Ni–Ga	973	7.2145	0.1518	0.2327	246,038
Ni–Ge	973	6.9477	0.1172	0.2396	591,570
Ni–Ge	997	6.9590	0.1193	0.2388	584,914
Ni–Si	923	6.7537	0.1062	0.2276	928,238
Ni–Si	1048	6.7965	0.1187	0.2276	903,279
Ni–Ti	965	6.8799	0.0978	0.2300	575,618
Ni–Ti	993	6.8758	0.1005	0.2300	573,622

reported in their Fig. 4 are too low, and that the lattice constants they measured are close to their equilibrium values. Taking all these factors into account leads to the values of G''_m shown in Table 4.

Calculations of σ

The parameters needed to calculate σ for all the alloys in the contexts of the TIDC and LSW theories are summarized in Tables 5 and 6, respectively. The values of σ are presented in Table 7 and are calculated from those in Tables 5 and 6 after compensating for their variances (i.e., the squares of the standard deviations shown in the two tables). In some cases, e.g., the data of Wimmel and Ardell [16] on the kinetics of solute depletion in Ni–Ga alloys shown in Fig. 4b, the variances are very large, producing the large standard deviations in the individually calculated values of σ seen in Tables 5 and 6. In such cases the contributions of these particular measurements to the weighted average values of σ presented in Table 7 are relatively small.

The estimated errors in Table 7 are very conservative, because there are many other factors that can affect the calculations. These include the exponent n in the TIDC theory and the equilibrium concentrations of both phases. Additionally, there is some flexibility in choosing the thermodynamic model used to calculate G''_m, and the reliability of the models themselves. With regard to the models selected, the curvatures of the Gibbs free energy of mixing of the Ni–Al solid solution calculated using the model of Du and Clavaguera [20] are about 25% larger than those from the model of Ansara et al. [19]. This would produce comparably larger values of σ. The model of Bellen et al. [27] of the Ni–Ti solid solution yields values of G''_m only slightly smaller than obtained from the model of De Keyzer et al. [30]. Matsumoto et al. [33] modeled the binary Ni–Ti phase diagram as part of their assessment of the ternary Nb–Ni–Ti system. The values of G''_m from their model are roughly 6–7% smaller than those from the model of De Keyzer et al. [30], so the models predict curvatures of the free energy of mixing that agree quite well. The values of σ reported in Table 7 for Ni–Al, Ni–Ga, Ni–Ge, and Ni–Ti alloys can therefore be considered to be as reliable as current analysis allows.

Unfortunately, the consistency among various models of the Ni–Al and Ni–Ti thermodynamics is not found for Ni–Si alloys. The model of Tokunaga et al. [26], which has been used to calculate σ in Table 7, overestimates the β_1 (γ'-type) solvus, though it provides a better fit than the models of Lindholm and Sundman [25] or Du and Schuster [24]. The model of Miettinen [32] actually provides the best fit to the β_1 solvus. If the values of G''_m from any of these other models are used to calculate σ from the data on

Table 5 Rate constants $\kappa_T^{-1/n}$ and k_T used in the calculations of σ assuming validity of the TIDC theory. The capillary length, ℓ_T, is also shown

Alloy	T (K)	$\kappa_T^{-1/n}$ ($s^{1/n}$)	k_T (m^n/s)	$\ell_T(m)$	σ (mJ/m^2)
Ni–Al	898	0.17575 ± 0.00207	$7.6826 \pm 1.0685 \times 10^{-26}$	7.6583×10^{-12}	22.33 ± 1.31
Ni–Al	988	0.04237 ± 0.00181	$2.1414 \pm 0.0874 \times 10^{-24}$	7.2860×10^{-12}	19.52 ± 0.90
Ni–Ga	901	0.07591 ± 0.00238	$5.3048 \pm 0.0333 \times 10^{-24}$	6.9054×10^{-12}	11.19 ± 0.35
Ni–Ga	973	0.01975 ± 0.00860	$1.8441 \pm 0.4633 \times 10^{-23}$	3.0754×10^{-12}	4.51 ± 2.02
Ni–Ga	973	0.02036 ± 0.01678	$2.6205 \pm 0.1263 \times 10^{-23}$	3.6899×10^{-12}	5.41 ± 4.46
Ni–Ge	973	0.02838 ± 0.01116	$2.3645 \pm 0.2120 \times 10^{-23}$	9.2491×10^{-12}	51.48 ± 20.34
Ni–Ge	973	0.06693 ± 0.00818	$2.9372 \pm 0.1520 \times 10^{-23}$	2.3890×10^{-11}	132.97 ± 16.50
Ni–Ge	973	0.03137 ± 0.01886	$2.9543 \pm 0.3972 \times 10^{-23}$	1.1226×10^{-11}	62.48 ± 37.72
Ni–Ge	997	0.01887 ± 0.00462	$6.2568 \pm 0.3266 \times 10^{-23}$	9.2473×10^{-12}	49.71 ± 12.22
Ni–Ge	997	0.03114 ± 0.00609	$5.6927 \pm 0.3231 \times 10^{-23}$	1.4671×10^{-11}	78.87 ± 15.55
Ni–Ge	997	0.04148 ± 0.01320	$5.8055 \pm 0.4923 \times 10^{-23}$	1.9701×10^{-11}	105.91 ± 33.91
Ni–Si	923	0.07113 ± 0.01370	$1.3063 \pm 0.0492 \times 10^{-24}$	1.2011×10^{-11}	104.84 ± 20.25
Ni–Si	923	0.04321 ± 0.01694	$1.4991 \pm 0.0375 \times 10^{-24}$	7.7182×10^{-12}	66.73 ± 26.42
Ni–Si	923	0.06530 ± 0.01651	$1.1880 \pm 0.0382 \times 10^{-24}$	1.0606×10^{-11}	92.57 ± 23.44
Ni–Si	923	0.06597 ± 0.00663	$1.4898 \pm 0.0551 \times 10^{-24}$	1.1754×10^{-11}	102.60 ± 10.43
Ni–Si	1048	0.00842 ± 0.00099	$1.2740 \pm 0.0179 \times 10^{-22}$	9.2661×10^{-12}	70.15 ± 8.24
Ni–Ti	965	0.07558 ± 0.00376	$2.5971 \pm 0.0617 \times 10^{-23}$	9.4801×10^{-12}	57.27 ± 2.86
Ni–Ti	993	0.04297 ± 0.01124	$1.1684 \pm 0.0720 \times 10^{-22}$	1.0421×10^{-11}	60.39 ± 15.88
Ni–Ti	993	0.07203 ± 0.00795	$2.3226 \pm 0.2215 \times 10^{-23}$	8.6027×10^{-12}	49.85 ± 5.89
Ni–Ti	993	0.09962 ± 0.01152	$2.5075 \pm 0.2665 \times 10^{-23}$	1.2305×10^{-11}	71.30 ± 8.89

Table 6 Rate constants $\kappa^{-1/3}$ and k used in the calculations of σ assuming validity of the LSW theory. The capillary length, ℓ, is also shown

Alloy	T (K)	$\kappa^{-1/3}$ ($s^{1/3}$)	k (m^3/s)	$\ell(m)$	σ (mJ/m^2)
Ni–Al	898	0.08675 ± 0.00207	2.1379 ± 0.2565 × 10^{-30}	1.1175 × 10^{-11}	31.08 ± 1.45
Ni–Al	988	0.02599 ± 0.00181	7.2526 ± 0.4011 × 10^{-29}	1.0840 × 10^{-11}	27.70 ± 2.00
Ni–Ga	901	0.03932 ± 0.00111	2.3605 ± 0.1756 × 10^{-29}	1.1278 × 10^{-11}	17.19 ± 0.645
Ni–Ga	973	0.01178 ± 0.00860	7.7129 ± 1.7371 × 10^{-29}	5.0158 × 10^{-12}	6.92 ± 3.10
Ni–Ga	973	0.01194 ± 0.01678	1.4188 ± 0.0385 × 10^{-28}	6.2276 × 10^{-12}	8.59 ± 7.31
Ni–Ge	973	0.01830 ± 0.00709	5.1503 ± 0.3141 × 10^{-28}	1.4667 × 10^{-11}	76.39 ± 29.66
Ni–Ge	973	0.04050 ± 0.00479	7.9805 ± 0.5108 × 10^{-28}	3.7565 × 10^{-11}	195.67 ± 23.51
Ni–Ge	973	0.01979 ± 0.01222	6.8513 ± 0.9493 × 10^{-28}	1.7449 × 10^{-11}	90.89 ± 56.32
Ni–Ge	997	0.01051 ± 0.00250	2.4848 ± 0.1930 × 10^{-27}	1.4240 × 10^{-11}	71.51 ± 17.13
Ni–Ge	997	0.01746 ± 0.00311	2.1185 ± 0.1830 × 10^{-27}	2.2430 × 10^{-11}	112.66 ± 20.90
Ni–Ge	997	0.02304 ± 0.00728	2.1478 ± 0.2285 × 10^{-27}	2.9721 × 10^{-11}	149.28 ± 47.25
Ni–Si	923	0.03214 ± 0.00619	1.0621 ± 0.0508 × 10^{-28}	1.5219 × 10^{-11}	126.98 ± 24.53
Ni–Si	923	0.01928 ± 0.00774	1.1148 ± 0.0530 × 10^{-28}	9.2797 × 10^{-12}	77.43 ± 31.10
Ni–Si	923	0.02927 ± 0.00759	1.0763 ± 0.0128 × 10^{-28}	1.3923 × 10^{-11}	116.17 ± 30.12
Ni–Si	923	0.02976 ± 0.00306	1.1102 ± 0.0414 × 10^{-28}	1.4303 × 10^{-11}	119.34 ± 12.34
Ni–Si	1048	0.00542 ± 0.00077	1.4558 ± 0.0593 × 10^{-26}	1.3243 × 10^{-11}	95.83 ± 13.70
Ni–Ti	965	0.04273 ± 0.00231	6.7761 ± 1.0422 × 10^{-29}	1.7421 × 10^{-11}	96.36 ± 7.17
Ni–Ti	993	0.02147 ± 0.00523	7.3544 ± 0.3924 × 10^{-28}	1.9380 × 10^{-11}	104.71 ± 25.57
Ni–Ti	993	0.03560 ± 0.00360	5.8047 ± 0.4517 × 10^{-29}	1.3784 × 10^{-11}	74.48 ± 7.77
Ni–Ti	993	0.03425 ± 0.00658	4.4362 ± 0.2509 × 10^{-29}	1.2126 × 10^{-11}	65.51 ± 12.85

Table 7 Calculated values of the interfacial free energies, σ, of the γ/γ'-type interfaces in all five alloys

Alloy	σ (mJ/m^2)—TIDC	σ (mJ/m^2)—LSW
Ni–Al	20.42 ± 1.05	29.92 ± 1.66
Ni–Ga	10.96 ± 0.60	16.70 ± 1.09
Ni–Ge	74.98 ± 17.74	110.40 ± 25.01
Ni–Si	84.33 ± 13.00	109.18 ± 17.85
Ni–Ti	56.16 ± 4.87	83.97 ± 9.56

coarsening, the results are much smaller in magnitude. The results of calculations of σ using the thermodynamic models of Du and Schuster [24] and Miettinen [32] are shown in Table 8. It is evident that the values of G''_m are much smaller than those obtained from the model of Tokunaga et al. [26] (see Table 4), yielding values of σ that are about 1/2 to 2/3 those shown in Fig. 7. This is a huge discrepancy, which cannot be reconciled without independent measurements of σ, or clear confirmation that one of the thermodynamic models is superior to the other.

Discussion

It is not evident from the numbers in Table 7, but the influence of non-ideality of the solid solutions on the calculated values of σ is quite large, ranging from a factor of about 4 for Ni–Ga alloys to over a factor of 10 for Ni–Si alloys. For the reader who is not familiar with the data on coarsening of the γ'-type precipitates in these alloys, it should be obvious on viewing Figs. 5, 6, 7, 8, 9, 10, and 11 that there is no effect of initial alloy concentration on the kinetics of coarsening, which means that there is no effect of f_e either. For some of the data shown f_e varies by as much as a factor of 10, so if any of the theories noted in the review articles cited [35–38] were correct, the effect on kinetics would have to be considered in the calculations of σ. The TIDC theory completely obviates this issue since no effect of f_e is predicted.

In assessing the reliability of the calculated values of σ, independently measured or calculated values would be immensely helpful. Unfortunately, except for the important Ni–Al alloy system such calculations have not been made. Since the γ/γ' interface is so technologically important, the Ni(Al)/Ni_3Al interfacial energy has been estimated by several groups using atomistic calculations. All these calculations assume that pure Ni is in equilibrium with stoichiometric Ni_3Al, so the calculated values represent upper limits of the energies at 0 K. The first such calculation was that of Farkas et al. [73] using embedded atom potentials. They calculated $\sigma \approx 22$ mJ/m^2. Price and Cooper [74] used a different atomistic method and obtained values of 25 or 63 mJ/m^2, with the differences due to the treatment of magnetic effects. Mishin [40] used newer embedded atom potentials and found that σ varied depending on the orientation of the interface, being lowest for the (111)

Table 8 Calculated values of the interfacial free energy of the Ni(Si)/Ni_3Si interface using the thermodynamic models of Du and Schuster [24] and Miettinen [32]

Model	T (K)	G''_m (J/mol)	σ (mJ/m^2)—TIDC	σ (mJ/m^2)—LSW
Miettinen [32]	923	443,870	53.66 ± 8.28	69.61 ± 11.39
	1048	435,258		
Du and Schuster [24]	923	593,977	40.50 ± 6.24	52.36 ± 8.56
	1048	572,441		

interface (12 mJ/m^2) and highest for the (100) interface (46 mJ/m^2). Somewhat similar results were obtained by Costa et Silva et al. [34], whose first-principles calculations also produced anisotropic values of σ, namely 39.6 and 63.8 mJ/m^2 for the (100) and (110) interfaces, respectively. On comparing these theoretical estimates with the experimental results in this work, two factors need to be considered. The first is the theoretically predicted anisotropy of σ, and the second is effect of temperature, since the values of σ obtained from the data on coarsening are values representative of $T \gg 0$ K.

There is no experimental evidence for an orientation dependence of the interfacial energy in Ni-base γ/γ' alloys. Indeed, there is overwhelming evidence that the shapes of γ'-type precipitates are governed uniquely by the competition between elastic and interfacial energies. Review articles by Doi [75] and Fratzl et al. [76] show transmission electron micrographs of γ' precipitates in ternary alloys with compositions deliberately selected to alter the elastic mismatch between the precipitate and matrix phases. The shapes of the γ' precipitates are invariably spherical when the elastic mismatch is close to zero no matter how large the precipitates are, with no evidence whatsoever of faceting. There is currently no explanation for the discrepancy with Mishin's atomistic calculations. Regarding the effect of temperature, the values of σ would be expected to decrease as T increases from 0 K. The interfacial energy would also decrease on taking the chemistry of the precipitates into account. The apparent agreement among the theoretically calculated values of σ for the Ni(Al)/Ni_3Al interface and those seen in Table 7 must clearly be regarded as fortuitous.

It is legitimate to question whether a constant value of σ during coarsening is physically meaningful if the width of the interface is allowed to vary, as specified by Eq. 10. The width of the interface is a manifestation of the gradient energy, χ, in these alloy systems, and as demonstrated nicely in the paper by Lass et al. [77], δ is expected to increase as χ increases because of the energy penalty the system must pay if the interface is relatively sharp and χ is relatively large. Since σ is proportional to χ [78], the interfacial energy should also vary as δ varies. Such considerations would appear to obviate the basis of the TIDC-based analysis of the data in this paper. A solution to this apparent conundrum lies in a simple relationship between σ, χ and δ derived in Appendix 2. The relationship is given by the equation

$$\sigma \approx C\chi\frac{\left(X_{\gamma'} - X_{\gamma}\right)^2}{\delta}, \tag{25}$$

where C is a numerical constant.

Inspection of Eq. 25, recalling Eq. 10, indicates that σ cannot remain approximately constant as r (hence δ) increases unless the increase in size is accompanied by an increase in χ. Over the range of average particle sizes of the precipitates analyzed in this work, Eq. 10 predicts that δ should increase by factors of about 1.4 (Ni–Ga), 1.7 (Ni–Al, Ni–Ge, and Ni–Ti), and 2 (Ni–Si). The question therefore is whether there is any evidence that χ can possibly increase by a comparable amount in order that the values of σ shown in Table 7 remain approximately constant, at least over the ranges of temperatures of the experiments on coarsening.

There are two studies that support the idea that χ can increase as r (hence δ) increases. One is found in a recent paper by Hoyt [79], who investigated the thermodynamic equilibrium conditions for Cu-rich droplets in the Cu–Pb system using molecular dynamics simulations. Hoyt compared the gradient energies of planar and curved solid Cu–liquid Pb interfaces and found that χ at 1000 K for a droplet 5.3 nm in diameter is 1.27×10^{-10} J/m compared to 2.18×10^{-10} J/m for a planar Cu–Pb interface. The factor of $\sim$1.7 increase in χ is comparable to the increases in δ predicted by Eq. 10. This is a fortuitous, but nevertheless encouraging, result.

The other piece of evidence is found in Fig. 4 of a paper by Booth-Morrison et al. [80] on the coarsening of γ' precipitates in a ternary Ni–Al–Cr alloy. They measured concentration profiles across interfaces using atom-probe tomography at aging times of 1, 4, and 4096 h. The maximum absolute values of the concentration gradients of Al and Ni, $|dX_{Al}/dy|_{max}$ and $|dX_{Ni}/dy|_{max}$ in the notation used in Appendix 2, at 1 h of aging are a factor of 1.5 to 1.6 larger than those at 4096 h of aging. Assuming that these gradients are proportional to the average gradients, $\langle dX_{Al}/dy\rangle$ and $\langle dX_{Ni}/dy\rangle$, respectively (see Appendix 2), δ must increase as the interfacial concentration gradients

increase, with increases comparable to those of the maximum gradients. The computer simulations of Hoyt [79] and the measurements of Booth-Morrison et al. [80] do not prove conclusively that χ varies with r, but their work provides clear evidence that it is reasonable to assume that σ can remain approximately constant while δ increases.

The interfacial free energies calculated using the TIDC theory are approximately 2/3 those calculated using the LSW theory, with the exception of the Ni–Si system where the ratio is $\sim$3/4. The reason for the smaller difference in Ni–Si alloys is that the data on the 2 longest aging times in the results of Cho and Ardell [55] were omitted in the TIDC analysis but used in the LSW analysis. A similar treatment was accorded the data on the Ni–Ge alloys, but only one point was omitted and its omission has only a relatively small effect on σ calculated using the TIDC theory.

The rationale stated earlier for excluding the data at longer aging times is that $\langle r \rangle$ exceeds $r_T > \delta\tilde{D}/\tilde{D}_I \approx 80$ nm. There are no data on diffusion in Ni_3Si, so it is not possible to estimate $\tilde{D}_I$, which is expected to be slightly larger than $\tilde{D}_{Ni_3Si}$ though of course smaller than chemical diffusion in the matrix. It is, nevertheless, instructive to see if the data on chemical diffusion in Ni–Ge alloys can be used to rationalize the exclusion of the long-time data in this system. Chemical diffusion coefficients in both Ni_3Ge and the Ni–Ge solid solution have been measured by Komai et al. [81]. Using the empirical equations reported for the Ni–Ge solid solution (10% Ge) and Ni_3Ge (23.5% Ge), $\tilde{D}_{Ni-10\%\,Ge} = 6.29 \times 10^{-5}\exp(-233,000/RT)$ and $\tilde{D}_{Ni_3Ge} = 9.03 \times 10^{-5}\exp(-248,000/RT)$, respectively, the ratio $\tilde{D}/\tilde{D}_I$ is about 4.5 at 700 °C. With $\delta = 2$ nm the transition radius r_T is $r_T \approx 9$ nm. This is about a factor of 10 smaller than the assumed transition radius, but it should be kept in mind that chemical diffusion in the Ni–Ge matrix is strongly dependent on concentration. Judging from the data of Komai et al. [81] reported in their Fig. 10 chemical diffusion in an alloy containing $\sim$11.8% Ge, which is within the range of equilibrium concentrations in the matrix of the aged Ni–Ge alloys (see Table 4), $\tilde{D}$ would increase by a factor of 3–4, leading to a concomitant increase in r_T by the same amount for this value of δ. Whereas these arguments do not fully justify the exclusion of data for which $\langle r \rangle > r_T$, they provide sensible rationale for doing so.

The other factor involved in the transition from TIDC to LSW kinetics is the behavior of the PSDs. In principle, when the kinetics of coarsening is controlled by diffusion in the matrix phase the PSDs are broader than predicted by the original LSW theory owing to the effect of volume fraction [35–38]. In practice, experimental PSDs tend to be broader than the LSW PSD anyway, even if there is no effect of f_e on the kinetics. Given the relatively poor statistics involved in the measurements of the PSDs, it is impossible to characterize the PSDs discussed in this work accurately enough to distinguish any possible mechanism that might be responsible for broadening. In other words, any expected changes in the shape of the PSDs in the transition from TIDC to LSW kinetics are not detectable.

It is natural to conjecture about the relative magnitudes of σ for the different alloy systems. As noted some time ago [10] interfacial free energies in γ/γ' alloys are dominated by second- and higher-order neighbor interactions. It is reasonable to conclude that these interactions for the covalent Group IV elements Si and Ge are stronger than those for the Group III elements Al and Ga. This is consistent with the larger Ni(Si)/Ni_3Si and Ni(Ge)/Ni_3Ge interfacial energies compared to the Ni(Al)/Ni_3Al and Ni(Ga)/Ni_3Ga interfacial energies. Moreover, since bond energies tend to decrease as the atomic number increases, i.e., bonding in Ge and Ga is weaker than bonding in Si and Al, respectively, the Ni(Al)/Ni_3Al interfacial energy should be larger than the Ni(Ga)/Ni_3Ga energy, and the Ni(Si)/Ni_3Si energy should exceed the Ni(Ge)/Ni_3Ge interfacial energy. These expectations are confirmed by the values of σ seen in Table 7, with the sole exception for the relative interfacial energies in the Ni–Si and Ni–Ge alloys calculated using the LSW analysis of the data, which produces roughly equal values of σ in the two systems.

The only independent measurements of thermodynamic quantities that support this argument are those of Martosudirjo and Pratt [82], who report that the heat of solution of Ge in Ni at 836 K is about 13 times larger than that of Ga at 778 K. These measurements indicate that first nearest-neighbor interactions in Ni–Ge are significantly larger than in Ni–Ga, and by inference the higher-order interactions are also larger. It is not possible to extend this argument to the transition metal Ti, but since the valence state of Ti is generally larger than that of Al and Ga it would be expected that larger values of σ for the Ni(Ti)/Ni_3Ti system would be observed, which is also consistent with the data in Table 7.

Given the uncertainties in the magnitudes of all the parameters associated with these estimates, it is concluded that the TIDC theory successfully describes the data on coarsening in all five alloys. The consideration of bonding also provides justification for the validity of the thermodynamic model of Tokunaga et al. [26] in describing the thermodynamics of the Ni–Si alloy system. The other two thermodynamic models used to calculate σ in Table 8 yield magnitudes that appear to be too small. Whether the values of σ obtained using the TIDC-based analyses are more "accurate" than those obtained from the LSW-based analyses awaits confirmation. This will come when atomistic calculations can properly account for the equilibrium compositions of the γ and γ'-type phases at temperatures in

the range 800–1000 K, as well as the absence of an orientation dependence of σ in the absence of elastic mismatch.

Acknowledgements I am very grateful to Dr. Nathalie Dupin, Calcul Thermodynamique, for her help in unraveling the mysteries (to me) of thermodynamic assessments of the Ni–Al phase diagram and, by inference, others. I also thank Professor Y.Q. Liu, China University of Geosciences, Beijing, for her help in dealing with the thermodynamic assessment of the Ni–Ge phase diagram. Professor Vidvuds Ozolins, UCLA, provided very helpful discussions of bonding in the five alloys, and his valuable insights are greatly appreciated.

Appendix 1

The general expression for $G_{m,mag}$ is [83]

$$G_{m,mag} = RTf(\tau)\,\ell n(\beta+1), \tag{26}$$

where β is the average magnetic moment in the alloy, expressed as Bohr magnetons, $\tau = T/T_C$ and $f(\tau)$ is given by the equation [84]

$$f(\tau) = \frac{-0.4269}{\tau^5}\left\{\frac{1}{10}+\frac{1}{315\tau^{10}}+\frac{1}{1500\tau^{20}}\right\}, \tag{27}$$

where the constant 0.4269 is operative for f.c.c. alloys. Allowing for the possibility that β depends on X, as well as τ via the dependence of T_C on X, the expression for $G''_{m,mag}$ is

$$\frac{G''_{m,mag}}{RT} = \frac{f(\tau)}{(\beta+1)}\left\{\beta'' - \frac{1}{(\beta+1)}(\beta')^2\right\} + \frac{2}{(\beta+1)}\beta' f'(\tau) + f''(\tau)\ell n(\beta+1) \tag{28}$$

where the primes again denote derivatives with respect to composition,

$$f'(\tau) = \frac{0.4269\tau'}{\tau^6}\left\{\frac{1}{2}+\frac{1}{21\tau^{10}}+\frac{1}{60\tau^{20}}\right\} \tag{29}$$

and

$$f''(\tau) = \frac{0.4269}{\tau^6}\left[\left\{\frac{1}{2}+\frac{1}{21\tau^{10}}+\frac{1}{60\tau^{20}}\right\}\tau'' - \frac{(\tau')^2}{\tau}\left\{3+\frac{16}{21\tau^{10}}+\frac{13}{30\tau^{20}}\right\}\right]. \tag{30}$$

The derivatives of τ are given by the equations

$$\tau' = -\frac{\tau^2 T'_C}{T} \tag{31}$$

and

$$\tau'' = \frac{\tau^2}{T}\left\{\frac{2\tau(T'_C)^2}{T} - T''_C\right\}. \tag{32}$$

Most of the thermodynamic assessments cited in this paper do not include detailed estimates of $G_{m,mag}$, even though its existence is noted. An exception is the model of Tokunaga et al. [26]. They represent the variations of β and T_C by the equations

$$\beta = 0.52(1-X) \tag{33}$$

and

$$T_C = 633(1-X) - 3872X(1-X), \tag{34}$$

respectively. On performing the necessary differentiations and substituting the results into Eqs. 29 to 32, then into Eq. 28, the values of G''_m for the aging temperatures of 650 and 775 °C are negative and very small, −416 and −106 J/mol, respectively. Since the variations of T_C and β for all the alloys are expected to be similar, it is safe to conclude that the magnetic contributions can be ignored.

Appendix 2

Following Cahn and Hilliard [78, 85], the change in molar free energy, ΔG_m, accompanying a composition gradient dX/dy, can be expressed as[4]

$$\Delta G_m = \chi V_m\left(\frac{dX}{dy}\right)^2 \tag{35}$$

and the interfacial energy is given by the equation

$$\sigma = \int_{X_\alpha}^{X_\beta}\left(\frac{\chi\Delta G_m}{V_m}\right)^{1/2} dX \tag{36}$$

Substitution of Eq. 35 into Eq. 36 gives the result

$$\sigma = \chi\int_{X_\gamma}^{X_{\gamma'}}\left(\frac{dX}{dy}\right)dX \tag{37}$$

The average value of dX/dy can be obtained from the equation

$$\left\langle\frac{dX}{dy}\right\rangle = \frac{\int_{X_\gamma}^{X_{\gamma'}}\left(\frac{dX}{dy}\right)dX}{\int_{X_\gamma}^{X_{\gamma'}}dX} = \frac{\int_{X_\gamma}^{X_{\gamma'}}\left(\frac{dX}{dy}\right)dX}{X_{\gamma'}-X_\gamma}, \tag{38}$$

so that σ can be expressed as

$$\sigma = \chi(X_{\gamma'}-X_\gamma)\left\langle\frac{dX}{dy}\right\rangle \tag{39}$$

On expressing the average gradient across the interface as

[4] The gradient energy χ differs by a factor of 2 in various treatments of decomposition from supersaturated solid solution. These distinctions are ignored here because the magnitude of χ is immaterial to the discussion in this paper.

$$\left\langle \frac{dX}{dy} \right\rangle \approx \frac{C\left(X_{\gamma'} - X_{\gamma}\right)}{\delta}, \tag{40}$$

where C is a numerical constant, we arrive at the simple expression for σ given by eq. (25).

In the derivation of Eq. 39 the gradient energy has been taken as constant. In fact χ generally varies with composition (see [86] for a representative evaluation), but for the relatively small difference between X_{γ} and $X_{\gamma'}$ ($\sim 12\%$) the assumption of constancy of χ in the integral, Eq. 36, is reasonable. There is also a contribution to χ from the gradient in long-range order [87], but in phase-field simulations the magnitude of this contribution generally varies from 10 [87] to ~ 400 times [88] smaller than the chemical contribution.

References

1. Lifshitz IM, Slyozov VV (1961) J Phys Chem Solids 19:35
2. Wagner C (1961) Zeitschrift Fur Elektrochemie 65:581
3. Greenwood GW (1956) Acta Metall 4:243
4. Todes OM, Khrushchov VV (1947) Zh Fiz Khim 21:301
5. Ardell AJ, Nicholson RB (1966) Acta Metall 14:1295
6. Ardell AJ (1967) Acta Metall 15:1772
7. Ben Israel DH, Fine ME (1963) Acta Metall 11:1051
8. Marian V (1937) J Phys Radium 8:313
9. Ardell AJ (1968) Acta Metall 16:511
10. Ardell AJ, Nicholson RB (1966) J Phys Chem Solids 27:1793
11. Chaix JM, Eustathopoulos N, Allibert CH (1986) Acta Metall 34:1589
12. Trivedi RK (1975) In: Lectures on the theory of phase transformations, AIME, p 51
13. Calderon HA, Voorhees PW, Murray JL, Kostorz G (1994) Acta Metall Mater 42:991
14. Rastogi PK, Ardell AJ (1969) Acta Metall 17:595
15. Kim DM, Ardell AJ (2004) Metall Mater Trans A 35A:3063
16. Wimmel J, Ardell AJ (1994) J Alloys Compd 205:215
17. Kim DM, Ardell AJ (2003) Acta Mater 51:4073. doi:10.1016/S1359-6454(03)00227-1
18. Wimmel J, Ardell AJ (1994) Mater Sci Eng A 183:169
19. Ansara I, Dupin N, Lukas HL, Sundman B (1997) J Alloys Compd 247:20
20. Du Y, Clavaguera N (1996) J Alloys Compd 237:20
21. Zhang F, Chang YA, Du Y, Chen SL, Oates WA (2003) Acta Mater 51:207. doi:10.1016/s1359-6454(02)00392-0
22. Yuan WX, Qiao ZY, Ipser H, Eriksson G (2004) J Phase Equilib Diffusion 25:68. doi:10.1361/10549710417696
23. Liu YQ, DJ Ma, Du Y (2010) J Alloys Compd 491:63. doi:10.1016/j.jallcom.2009.11.036
24. Du Y, Schuster JC (1999) Metall Mater Trans A 30A:2409
25. Lindholm M, Sundman B (1996) Metall Mater Trans A 27A:2897
26. Tokunaga T, Nishio K, Ohtani H, Hasebe M (2003) Calphad 27:161. doi:10.1016/s0364-5916(03)00049-x
27. Bellen P, Kumar K, Wollants P (1996) Zeitschrift Fur Metallkunde 87:972
28. Dupin N, Ansara I, Sundman B (2001) Calphad 25:279
29. Schuster J (2006) Intermetallics 14:1304. doi:10.1016/j.intermet.2005.11.027
30. De Keyzer J, Cacciamani G, Dupin N, Wollants P (2009) Calphad 33:109. doi:10.1016/j.calphad.2008.10.003
31. Du Y, CY He, Schuster JC, Liu SH, Xu HH (2006) Int J Mater Res 97:543
32. Miettinen J (2005) Calphad 29:212
33. Matsumoto S, Tokunaga T, Ohtani H, Hasebe M (2005) Mater Trans 46:2920
34. Costa e Silva A, Agren J, Clavaguera-Mora MT et al (2007) Calphad 31:53. doi:10.1016/j.calphad.2006.02.006
35. Ardell AJ (1988) In: Lorimer GW (ed) Phase transformation '87. The Institute of Metals, London, p 485
36. Baldan A (2002) J Mater Sci 37:2171. doi:10.1023/A:1015388912729
37. Voorhees PW (1992) Annu Rev Mater Sci 22:197
38. Jayanth CS, Nash P (1989) J Mater Sci 24:3041. doi:10.1007/BF01139016
39. Harada H, Ishida A, Murakami Y, Bhadeshia H, Yamazaki M (1993) Appl Surf Sci 67:299
40. Mishin Y (2004) Acta Mater 52:1451. doi:10.1016/j.actamat.2003.11.026
41. Sudbrack CK, Yoon KE, Noebe RD, Seidman DN (2006) Acta Mater 54:3199. doi:10.1016/j.actamat.2006.03.015
42. Srinivasan R, Banerjee R, Hwang JY et al (2009) Phys Rev Lett 102:086101. doi:10.1103/PhysRevLett.102.086101
43. Ardell AJ, Ozolins V (2005) Nat Mater 4:309. doi:10.1038/nmat1340
44. Fujiwara K, Horita Z (2002) Acta Mater 50:1571
45. Ikeda T, Almazouzi A, Numakura H, Koiwa M, Sprengel W, Nakajima H (1998) Acta Mater 46:5369
46. Janssen MMP (1973) Metall Trans 4:1623
47. Watanabe M, Horita Z, Sano T, Nemoto M (1994) Acta Metall Mater 42:3389
48. Ardell AJ (2010) Acta Mater 58:4325. doi:10.1016/j.actamat.2010.04.018
49. Ardell AJ, Kim DM, Ozolins V (2006) Zeitschrift Fur Metallkunde 97:295
50. Jayanth CS, Nash P (1990) Mater Sci Technol 6:405
51. Irisarri AM, Urcola JJ, Fuentes M (1985) Mater Sci Technol 1:516
52. Rastogi PK, Ardell AJ (1971) Acta Metall 19:321
53. Polat S, Chen H, Epperson JE (1989) Metall Trans A 20A:699
54. Ardell AJ (1995) Interface Sci 3:119
55. Cho J-H, Ardell AJ (1998) Acta Mater 46:5907
56. Ardell AJ (1970) Metall Trans 1:525
57. Kim DM, Ardell AJ (2000) Scripta Mater 43:381
58. Zener C (1955) Trans Am Inst Min Metall Engrs 203:619
59. Inden G (1975) Zeitschrift Fur Metallkunde 66:577
60. Miodownik AP (1977) Calphad 1:133
61. Redlich O, Kister AT (1948) Ind Eng Chem 40:345
62. Hashimoto K, Tsujimoto T (1978) Trans Jpn Inst Met 19:75
63. Ardell AJ (1994) In: Morral JE, Schiffman RS, Merchant SM (eds) Experimental methods of phase diagram determination. TMS, Warrendale, PA, p 57
64. Ma Y, Ardell AJ (2003) Zeitschrift Fur Metallkunde 94:972
65. Ikeda T, Nose Y, Korata T, Numakura H, Koiwa M (1999) J Phase Equilib 20:626
66. Oya Y, Suzuki T (1983) Zeitschrift Fur Metallkunde 74:21
67. Jia C, Ishida K, Nishizawa T (1994) In: Morral JE, Schiffman RS, Merchant SM (eds) Experimental methods of phase diagram determination. TMS, Pittsburgh, PA, p 31
68. Grune R (1988) Acta Metall 36:2797
69. Sinclair R, Leake JA, Ralph B (1974) Phys Status Solidi A 26:285
70. Vyskocil P, Pedersen JS, Kostorz G, Schonfeld B (1997) Acta Mater 45:3311
71. Kamara AB, Ardell AJ, Wagner CNJ (1996) Metall Mater Trans A 27A:2888
72. Sass SL, Mura T, Cohen JB (1967) Philos Mag 16:679

73. Farkas D, Decampos MF, Desouza RM, Goldenstein H (1994) Scripta Metall Mater 30:367
74. Price DL, Cooper BR (1996) In: Kaxiras E, Joannopoulos J, Vashishta P, Kalia RK (eds) Materials theory, simulations, and parallel algorithms, vol 408, MRS, p 463
75. Doi M (1996) Prog Mater Sci 40:79
76. Fratzl P, Penrose O, Lebowitz JL (1999) J Stat Phys 95:1429
77. Lass EA, Johnson WC, Shiflet GJ (2006) Calphad 30:42. doi:10.1016/j.calphad.2005.11.002
78. Cahn JW, Hilliard JE (1958) J Chem Phys 28:258
79. Hoyt JJ (2007) Phys Rev B 76:094102. doi:10.1103/PhysRevB.76.094102
80. Booth-Morrison C, Zhou Y, Noebe RD, Seidman DN (2010) Philos Mag 90:219. doi:10.1080/14786430902806660
81. Komai N, Watanabe M, Horita Z (1995) Acta Metall Mater 43:2967
82. Martosudirjo S, Pratt JN (1976) Thermochim Acta 17:183
83. Inden G (1981) Phys B & C 103:82
84. Hillert M, Jarl M (1978) Calphad 2:227
85. Cahn JW, Hilliard JE (1959) J Chem Phys 31:688
86. Asta M, Hoyt JJ (2000) Acta Mater 48:1089
87. Wang Y, Banerjee D, CC Su, Khachaturyan AG (1998) Acta Mater 46:2983
88. Wang JC, Osawa M, Yokokawa T, Harada H, Enomoto M (2007) Comput Mater Sci 39:871. doi:10.1016/j.commatsci.2006.10.014